In Silico Screening of Potential Antiviral Inhibitors against SARS-CoV-2 Main Protease

Kandhan Palanisamy
SRM Institute of Science and Technology
K. Rudharachari Maiyelvaganan
SRM Institute of Science and Technology
Shanmugasundaram Kamalakannan
SRM Institute of Science and Technology
Ramasamy Thilagavathi
Karpagam Academy of Higher Education: Karpagam University
Chelliah Selvam
Texas Southern University College of Pharmacy and Health Sciences
Muthuramalingam Prakash (prakashspm@gmail.com)
SRM University https://orcid.org/0000-0002-1886-7708

Research Article

Keywords: Main protease, Phytochemicals, ADME, Molecular dynamics, MM/PBSA.

Posted Date: March 24th, 2022

DOI: https://doi.org/10.21203/rs.3.rs-1330646/v1

Abstract

Respiratory illness due to SARS-CoV-2 emerged in 2019 and has a significant morbidity and mortality rate. The main protease (Mpro) is mainly responsible for the viral replications, which acts as a good drug target to inhibit SARS-CoV-2 related diseases. Chemical compounds obtained from various herbal plants are showing potent antiviral activity against numerous viral diseases. Initial screening was performed with the phytochemicals against Mpro using molecular docking. These result shows that there is a strong interaction exhibited between active sites (***His-41 and Cys-145***) of Mpro with chemical compounds. In addition, ADME prediction and Lipinski's rule of five calculations demonstrated that the selected compounds have potential drug-like properties. Further, molecular dynamics (MD) simulations were performed to understand the stability and structural changes of protein-ligand complexes for the top five compounds. MM/PBSA studies strongly suggested that compounds sitosterol, spinasterol, and asarinin form stable complexes with Mpro***.*** The most significant hot spot residues such as Thr-25, Met-49, Cys-145, Met-165, and Gln-189 have strongly interacted with the selected chemical compounds. Our calculations suggest that asarinin is the best inhibitor to the Mpro, which supports these candidates could be potent antiviral agents against SARS-CoV-2.

Introduction

The novel coronavirus (CoV) is a large family of viruses that causes more severe diseases such as severe acute respiratory syndrome (SARS in 2002-2003)[1] and the middle east respiratory syndrome (MERS in 2012) [2]. In December 2019, unknown pneumonia etiology emerged in Wuhan city, China. They observed symptoms such as dry cough, sore throat, dyspnea, and fever [3]. World Health Organization (WHO) declared that the Public Health Emergency of International Concern of COVID-19 is a pandemic disease by January 2020 [4]. The report states that SARS-CoV-2 is transmitted from bats to humans (i.e., Zoonotic). Later, SARS-CoV-2 transmissions from human to human was confirmed. It causes common cold, lung failure and leads to death [5]. The number of confirmed cases and deaths hikes significantly.

Coronaviruses belong to the subfamily of *Coronaviridae* and this subfamily includes four genera: i) Alpha coronavirus ii) Beta coronavirus iii) Gamma coronavirus iv) Delta coronavirus. The genome of the CoV is a single-stranded positive-sense RNA virus ((+)ssRNA), it has ~30 kilobase which encodes multiple structural and nonstructural proteins (Nsp1-16) [6]. The structural proteins are Spike *(S)*, Envelope (E), Membrane (M), and Nucleocapsid (N), whereas nonstructural polyproteins (Nsp) are responsible for viral functions, replications and survival in the host cell. Two proteases are 3-chymotrypsin-like-protease ($3CL^{pro}$) or main protease (Mpro) and Papain-like-protease (PL^{pro}) undergo autocleavage [7]. The report states that human angiotensin-converting enzyme 2 (hACE2) [8] is the key receptor and main entry point into the cell for SARS-CoV-2 [9]. The spike glycoprotein can bind and then fuse with human cells. Cryo-EM structure analysis has revealed a higher binding affinity for SARS-CoV-2 with human cells of ACE2 than SARS-CoV [10]. It concluded that SARS-CoV-2 has been possessed more transmissibility. Selvam et.al collected a review about targets, structures and inhibitors of SARS-CoV-1, which is helpful to understand

the inhibition mechanism of SARS-CoV-2 [11]. Recently, the mutation occurred in genomes of SARS-CoV-2, the most prevalent one is D614G. It is highly contagious than COVID-19 [12].

PLpro is responsible for the formations of Nsp1-3 and Mpro is responsible for the formations of Nsp4-16. Mpro causes the catalytic cleavage of 11 polyproteins, whereas PLpro causes only 3 polyproteins [13, 14]. Therefore, Mpro is playing a vital role in replications of viral polyproteins and hence it is a potential drug target to inhibit the SARS-CoV-2 [15, 16]. The active site of Mpro has a catalytic dyad, which is formed by His-41 and Cys-145 located in domain I (residues 8-101) and domain II (residues 102-184), respectively. The initial drug addressed in this pandemic is hydroxychloroquine (HCQ), which is an antiviral drug and is used in the treatment of malaria whose action is reinforced with the addition of azithromycin which was reported by the French research society [17]. Also, some of the other antiviral drugs have been used at present in both preventive as well as clinical drugs to treat COVID-19 [18]. Unfortunately, the efficacy and the alarming side-effects of these drugs are still not yet known.

Thus, the design and development of antiviral drug molecules to inhibit the functions of Mpro is essential. Naturally occurring [19] (i.e., herbal plants and foods) chemical compounds have antiviral activity, used as a medicine worldwide. Herbal plants and their phytoconstituents [20, 21] (extracted from stems, roots, seeds, barks, foods and flowers) result in potential antiviral activity for various diseases and enhance the immune system [22]. In this pandemic COVID-19, the screening of phytoconstituents and their derivatives are helpful into controlling the infections of SARS-CoV-2 [23]. CADD approaches are used to screen and identify the suitable antiviral drugs against Mpro of SARS-CoV-2 [24]. This method is affordable and decreases the time to discover a new antiviral drug candidate. Singam et al. screened the novel inhibitors which are obtained from the Nuclei of Bioassays, Ecophysiology, and Biosynthesis of Natural Products Database ($NuBBE_{DB}$) against the main protease [25]. Nhung and his co-workers studied the organosulfur compounds from garlic essential oil using gas chromatography-mass spectroscopy (GC-MS) and molecular docking techniques. They found that organosulfur compounds strongly interacted with the human ACE2 and Mpro of SARS-CoV-2 [26]. Kulkarni et al. selected the compounds from various essential oils and their docking analysis reveals that monoterpenes, terpenoid phenols, and phenyl propanoids have a stronger binding affinity with the spike receptor-binding domain (RBD) [27]. Gutierrez-Villagomez et al. studied the antiviral activity of alkamides and piperamides against the Mpro, RdRp (RNA dependent RNA polymerase), and ACE2. They calculated Lipinski's rule and ADME properties and evaluated the drug-like properties [28]. Recently, Wang et al. reported that the known anticancer drugs act as a potential inhibitor against SARS-CoV-2 Mpro. These results unravel the antiviral activity of naturally occurring compounds and strongly inhibit the replication process of proteases from SARS-CoV-2. Natural products and biocompatible ionic liquids strongly inhibit the Mpro activity.[29]

Even though there are numerous *in vivo* and *in vitro* approaches present in the design and development of potential antiviral inhibitors for SARS-CoV-2,[30] still there is a lack of evidence to understand the stability, structural changes and active site interactions of protein-ligand complexes. Our study is mainly focused to find potent antiviral drugs from natural compounds against Mpro and unravel the interaction mechanism of the same. For this, we have selected a series of natural products from various herbal

plants (non-toxic with no side effects) and performed docking-based virtual screening, molecular dynamics (MD) simulations and predicted ADME properties. In this work, computational investigations were carried out to evaluate the strong antiviral activity of phytochemicals against Mpro. Molecular-level insights will be helpful to design and develop natural inhibitors to control coronavirus-related disease. Our study will provide potential antiviral drug molecules to strongly inhibit the Mpro of SARS-CoV-2.

Materials And Methods

The crystallographic 3D structure of Mpro-apo (PDB ID: 6Y2E; resolution 1.75Å) [31] was retrieved from the protein data bank (www.rcsb.org). The PDB structure of Mpro was used for structure-based virtual screening and considered catalytic dyads of **His-41 and Cys-145** are the active sites of Mpro. The Mpro structure is displayed in Fig. 1. All the water molecules were removed and polar hydrogen atoms were added in protein preparation of Mpro. We have selected 25 chemical compounds from various herbal plants, and their coordinates were obtained from PubChem. 2D structures of all chemical compounds were shown in Fig. 2. All these structures were optimized with B3LYP/6-31+G* level of theory and their chirality was maintained. Subsequently, frequency calculations were carried out to confirm the energy minima in the potential energy surface (PES). All the compounds were optimized using Gaussian16 program [32]. The optimized compounds were considered as ligands for the screening process.

Molecular Docking Simulations

Molecular docking [33] was employed to predict the predominant binding modes of chemical compounds with SARS-CoV-2 Mpro. The best binding pose is considered as the lowest binding energy of the complex. Molecular docking was performed using *Autodock 4.2.6*, which is the most cited free software and has significant accuracy and performance [34]. The receptor of Mpro and ligands was prepared by adding atomic charges and atom types, then saved as PDBQT. The active sites of Mpro contain His-41 and Cys-145, which are covered by the grid box. The dimensions of an active site box were 60×126×126 $Å^3$ with a default grid spacing 0.375 Å was used for the docking. The selected 25 natural compounds from various herbal plants were docked with active sites of Mpro. The most stable ten binding conformations were obtained, and we investigated the interaction sites of protein-ligand complexes. The ADME properties (absorption, distribution, metabolism, and excretion) and Lipinski's rule of five (RO5) were calculated using SwissADME [35] and PKSCM [36]. The predicted properties include molecular weight, H-bond donors, H-bond acceptors, gastrointestinal (GI) absorption, rotatable bonds, hepatotoxicity and number of violations to rule of five. This will help to understand the drug-like properties of all chemical compounds.

Molecular Dynamics Simulations

MD simulations were performed to understand i) the relative stability and structural changes of Mpro-apo and Mpro bound with ligand (6Y2E + inhibitors) ii) binding free energy calculation and residue-ligand decomposition analysis. The protein-ligand complexes were placed in a cubic box with the dimensions of 97.5 Å × 97.5 Å × 97.5 Å. Mpro of SARS-CoV-2 was parameterized Amber99SB-ILDN force field [37], and the box was solvated with SPC/E water model. The ligands were parameterized with generalized amber

forcefield (GAFF) by using AmberTools18 [38] and ACPYPE [39] protocol. The partial atomic charges were assigned for ligands using the restrained electrostatic potential (RESP) method [40], which is computed by quantum chemical calculation at B3LYP/6-31+G(d,p) basis set. The counter ions were added to neutralize the system. The protein-ligand complexes were minimized by using the steepest descent algorithm. Further, the entire system was equilibrated under an NVT and NPT ensemble for 5 ns using velocity-rescaling and Berendsen coupling to maintain the temperature at 300 K and pressure at 1 bar, respectively. Periodic boundary condition (PBC) was applied for all three dimensions. The electrostatic interactions were calculated using the Particle Mesh Ewald (PME) method with a cutoff of 1.2 nm. We employed LINCS algorithm to constrain all bonds involving hydrogen atoms. In production run, all the system was simulated for 100 ns and the integration time step of 2 fs was used. MD simulations were performed by using Gromacs 2016.3 package [41]. The binding free energy was calculated between the Mpro and ligands using the g_mmpbsa tool [42]. The trajectories and structural conformations are visualized by using pyMOL [43] and VMD software [44].

Results And Discussion

Pandemic coronavirus causes severe respiratory illness, and to date none of the approved effective drugs are available. Currently used drugs causes adverse effect, and the inhibition mechanism is also not clear. Our study aims to identify the potential antiviral inhibitors for COVID-19. Mpro of SARS-CoV-2 cleaves more polyproteins than PLpro, and it plays a significant role in the process of viral replication. So Mpro acts as good drug target for inhibition of SARS-CoV-2. We unravel the chemical activity of various natural compounds with active sites of Mpro using CADD approaches [45]. *In silico* approaches will be helpful to get more insights about ligand interactions and structural changes of Mpro-complexes. In this study, we performed the two-step hierarchical virtual screening (HVS) of natural inhibitors against Mpro. First, molecular docking has been widely used to screen a large number of chemical compounds based on their binding affinity with active sites of Mpro. Next, the docked hits were subjected to MD simulations to understand the stability and structural changes of protein-ligand complexes. The final natural inhibitors were selected based on the MM-PBSA binding free energy calculation. Thereby, potent antiviral drugs can be identified to inhibit the SARS-CoV-2 Mpro.

Table 1

Top five docking hits and list of interacting residues.[a]

Compound No.	Compounds	Docking Score (kcal/mol)	H-bond residues	π-π interaction residues	Hydrophobic interactions
1.	β-Sitosterol	-10.6	Thr-26	His-41	Gly-143, Cys-145 and Glu-166
2.	α-Spinasterol	-10.3	Thr-24 and Thr-26	His-41	His-41, Cys-145 and Glu-166
3.	Lupeol	-9.5	Glu-166	NA	Thr-25, Thr-26, His-41, Asn-142 and Cys-145
4.	Glabridin	-8.0	Thr-25, Thr-190 and Thr-192	NA	Cys-145, Glu-166 and Gln-189
5.	Asarinin	-7.9	Ser-144 and His-163	NA	Leu-141, Cys-145, Glu-166 and Thr-190

[a] Docking score and their interactions are shown. NA = Not available

Molecular Docking

Molecular docking is an economical and fast pre-screening tool used to find out the ligand conformations, positions, orientations of binding sites, and binding affinities of drug molecules. We employed Autodock 4.2 to rapidly estimate the binding pose of Mpro with our selected ligands. The success rate of docking affinity for this package is 77%, according to the previous benchmark studies [46]. Huynh et al. reported that docking results of curcumin (-7.1 kcal/mol) and quercetin (-6.6 kcal/mol) with Autodock tools, these results are well correlated with our docking results and interacted with the active sites of Mpro [47]. Molecular docking is the first step of the HVS process. The predicted binding affinity (in kcal/mol) of the chemical compounds is considered as the antiviral activity against SARS-CoV-2 Mpro. The binding affinity of the top five docked hits and their type of residue interactions were provided in Table 1. The obtained binding affinity falls in the range from -4.7 to -10.6 kcal/mol. Five chemical compounds show a larger binding affinity to Mpro, where the range is more than -8.0 kcal/mol. Our docking results show stronger binding affinity compared with FDA-approved drugs, this will lead to the design of potent antiviral drugs against SARS-CoV-2 Mpro [48]. The complete details of selected compounds, respective sources, binding affinity, and their potential active site residue interactions are shown in supplementary information (SI) **Table S1.**

All chemical compounds [49–54] show good interaction with Mpro of SARS-CoV-2, especially β-sitosterol (sobatum), spinasterol, lupeol, glabridin and asarinin provide stronger binding affinity. Phytosterol components of β-sitosterol, and spinasterol acts as strong inhibitor based on the docking affinity of -10.6 and -10.3 kcal/mol, respectively. The protein-ligand complexes are stabilized by various types of

noncovalent interactions such as hydrogen bonding (H-bonding), salt bridges and hydrophobic interactions. The sitosterol group forms (O···H-N and H···O=C) two conventional H-bonding interactions with Thr-26 at 1.9 and 2.0 Å, respectively. Also, spinasterol forms two conventional H-bonding interactions with Thr-26 at the distances 2.0 Å. Lupeol, glabridin, and asarinin form H-bonded interactions with Glu-166 (2.1 Å), Thr-190 (2.1 Å) and His-163 (2.0 Å), respectively. In addition, these three compounds also interacted with the other residues such as Phe-294, Glu-240, Gln-110, His-246, Ile-152, Thr-111, Asp-203, Thr-292, Asp-295, Thr-292, and Lys-102. We anticipate that the compounds with binding energies greater than -7.0 kcal/mol, will have better antiviral activity to Mpro. The docked poses of protein-ligand complexes were shown in Fig. 3. These top five complexes are further subjected to MD simulations.

ADME Properties

ADMET profiles (absorption, distribution, metabolism, excretion and toxicity) were evaluated to understand the theoretical drug-like properties of our selected ligands. Lipinski's Rule of five (RO5) was assessed for all the compounds to identify the oral activity of drugs in humans [55]. The pharmacokinetic properties of all compounds were shown in Table 2. Some of the compounds violate MLogP but other properties of RO5 are in the acceptable range. The number of acceptable violations of Lipinski's rule is one. From the top five compounds, glabridin and asarinin exhibit high GI absorption and abides the RO5.

Table 2

ADME properties of selected phytochemicals.[a]

Compound Number	MW	nHB donors	nHB acceptors	nRotB	GI absorption	Hept.	nVio
1.	414.7	1	1	6	Low	No	1
2.	412.6	1	1	5	Low	No	1
3.	426.7	1	1	1	Low	No	1
4.	324.3	2	4	1	High	No	0
5.	354.3	0	6	2	High	No	0
6.	271.3	1	4	0	High	Yes	0
7.	314.2	3	7	1	High	No	0
8.	286.2	4	6	1	High	No	0
9.	246.2	1	4	1	High	Yes	0
10.	270.2	3	5	1	High	No	0
11.	287.3	2	5	0	High	Yes	0
12.	265.2	2	3	1	High	No	0
13.	285.3	0	3	4	High	Yes	0
14.	368.3	2	6	8	High	No	0
15.	304.2	5	7	1	High	No	0
16.	188.2	1	2	0	High	No	0
17.	204.3	0	0	0	Low	No	1
18.	204.3	0	0	4	Low	No	1
19.	222.3	1	1	0	High	No	0
20.	202.1	1	4	0	High	No	0
21.	222.2	0	4	4	High	No	0
22.	194.2	1	3	4	High	Yes	0
23.	136.2	0	0	1	Low	No	0
24.	177.2	2	4	5	High	No	0

[a] ADME properties of MW = Molecular weight (g/mol), nHB donors = number of H-bond donors, nHB acceptors = number of H-bond acceptors, nRotB = number of Rotatable bonds, GI absorption = Gastrointestinal absorption, Hept. = Hepatotoxicity and nVio = number of Lipinski's rule violation.

Compound Number	MW	nHB donors	nHB acceptors	nRotB	GI absorption	Hept.	nVio
25.	154.2	1	1	4	High	No	0

[a] ADME properties of MW = Molecular weight (g/mol), nHB donors = number of H-bond donors, nHB acceptors = number of H-bond acceptors, nRotB = number of Rotatable bonds, GI absorption = Gastrointestinal absorption, Hept. = Hepatotoxicity and nVio = number of Lipinski's rule violation.

Molecular Dynamics Simulations

The second step of HVS is the all-atom molecular dynamics simulations. There are several factors such as ligand protonation state, conformational changes, ions, and solvation effects are involved in the MD simulations. It is the refinement of docking results and to get more insight into the structural changes of the protein-ligand complexes. MD simulations were performed for the selected Mpro-complexes and Mpro-apo structure to understand the structure and stability of the complexes. This will be helpful in the optimization of screened ligands and rational drug design. Plots of total energies with time will be helpful to confirm the stability of the complexes during the entire MD simulations, which is shown in SI (**Fig. S1**). Root mean square deviation (RMSD) determines the stability of the protein-ligand system, Root mean square fluctuation (RMSF) depicts ligand effects on system fluctuations, Radius of gyration (R_g) shows compactness of global structure, and binding free energy (MM-PBSA) calculations are helpful to determine the binding affinity between protein and ligand. The per-residue decomposition analysis was also carried out to find contributions of specific amino acids on protein-ligand interactions. These free energy methods quantify the most efficient inhibitors and thereby lead to the design of Mpro inhibitors.

Structural stability of Mpro-apo and Mpro-complexes

The trajectories of Mpro-apo and Mpro-complexes are analyzed to understand the stability and conformational changes (RMSD) of the system. Results reveal that the backbone of Mpro-complexes attains stable deviations to entire MD simulations, and the average deviation is within 2Å. The ligands strongly interacted with Mpro and stabilized the protein-ligand complexes, RMSD plots were displayed in Fig. 4. In summary, the RMSD shows that ligands are strongly stabilized the protein during the overall MD simulations. In the first ~5 ns, lupeol was located in its initial position, after that the position was slightly changed. It forms stronger H-bonding interactions with Thr-26. All ligands remain in stable positions in the active sites of Mpro. The calculated RMSD backbone and C-alpha values for Mpro-apo and Mpro-complexes were shown in SI **(Table S2)**. The calculated residue-wise fluctuations (RMSF) for each amino acid of Mpro-apo and Mpro-complexes were shown in SI **(Fig. S2 and Table S2)**. RMSF of Mpro-apo is a baseline for comparing the fluctuations of ligand-bound Mpro. Complexes of sitosterol, spinasterol, lupeol, glabridin and asarinin reduced the fluctuations of Mpro residues. All the complexes increase the fluctuations of the N-terminus in domain III (residues 297-306). The structural comparisons of the initial Mpro and simulated Mpro of five complexes were displayed in Fig. 6-7. Average RMSD values informed all the ligands enhance the stability of complexes except glabridin. It increases local residue fluctuations

and reduces the stability of Mpro during the simulation time compared with other ligands. These results proved that sitosterol, spinasterol, glabridin, and asarinin strongly interacted with SARS-CoV-2 Mpro.

The secondary structure analysis shows the stability of protein residues. It is significantly revealed that residues 145-147 changes turn into the bend, as well residues 156-159 turns are slightly unfolded into bend structure. These results are helpful to understand the protein structure stability during the MD simulations. The secondary structures analyses were displayed in Fig. 5.

Binding mode analysis of ligands with Mpro

β-Sitosterol is structurally similar to cholesterol but has low absorption in the intestinal tract. β-Sitosterol is the major chemical component found in *Strobilanthes cusia* leaf, it has antiviral activity, immune system enhancing property, the cell proliferation inhibitory activity in human breast cancer cells and neutralizing cobra and viper venom [56–58]. Sitosterol belongs to the phytosterol group, which can induce the apoptosis process. In docking study, sitosterol forms H-bond with Thr-26, whereas in MD simulation shows that, the existence of salt bridge interactions with Mpro is favorable for stability of the complex. Thr-25, Leu-27, Met-49, Cys-145, Met-165, Pro-168 and Gln-189 residues of Mpro show polar and hydrophobic interactions with sitosterol. The hydrophobic amino acids cause van der Waals interactions between protein and ligands. The residues His-41, Cys-145, Met-165, Glu-166, and Gln-189 form non-conventional H-bonding interactions ~ 2.7 Å. These interaction sites were shown in Fig. 6A **and D.** Biologically active phytosterol compound of α-spinasterol is isolated from medical plant *Stegnosperma halimifolium.* It exhibits antiproliferative activity against the cervical cancer cell lines [59, 60]. Sterol compounds have shown stronger anticancer activities in human cancer cells. Thr-24 and Thr-26 form H-bonding interactions with Mpro, whereas in solvation study there are no H-bonding interactions exist. Hydrophobic interactions are involved with residues of His-41, Ser-46, Cys-145, Met-165, and Gln-189 **(**Fig. 6B **and E)**. The polar amino acids Ser-46, Cys-145, and Gln-189 form non-conventional H-bonding interactions. The hydrophobic side chains form van der Waals interactions with the sitosterol. Sitosterol and spinasterol have antiviral activity towards the Mpro of SARS-CoV-2.

Lupeol (also known as Fagarsterol) belongs to the triterpene group which is enriched in vegetables such as pepper, curcumin, strawberry, red grapes and some medicinal plants such as American ginseng and sea butter plant. It exhibits significant anti-inflammatory activity, which is equal to dexamethasone. The triterpene group directly inhibits the growth of human cancer cells under *in vivo* and *in vitro* systems. Lupeol act as a therapeutic and chemopreventive agent for the treatment of cancer and diabetes [61, 62]. Thr-26, His-41, Cys-145, and Glu-166 of Mpro made hydrophobic interactions with lupeol while Thr-26 forms a strong H-bond interaction (O···H-N) at the distance of 1.8 Å **(**Fig. 6C **and D)**. Licorice is widely available for herbal treatment used in Traditional Chinese Medicine (TCM). Glabridin is the main active compound, which has antiviral and antimicrobial activity [63, 64]. It is a type of isoflavonoid that interacts with residues Thr-26, Arg-188 forms non-conventional H-bond and with His-41 it forms π-π stacking interactions with Mpro **(**Fig. 7A **and C)**. Licorice is used for thousands of years in Chinese medicine as a life-enhancing agent [64]. Asarinin contains a furofuran ring which is extracted from the roots of *Asarum*

sieboldii. It exhibits cytotoxicity activity against the human ovarian cancer cells [65]. From docking, asarinin forms H-bonded interactions with Ser-144 and His-163. In MD simulations, asarinin exhibits a stronger binding affinity with Mpro and the interacting residues are Thr-25, His-41, Cys-44, Ser-46, Cys-145, His-164, Gln-189, Thr-190, and Gln-192 **(**Fig. 7B **and D)**. Asarinin forms stronger H-bond interactions with Thr-25, Gln-189, and Gln-192at the distance of 1.9 Å. The polar amino groups Cys-44, His-164, Gln-189, Thr-190, and Gln-192 form non-conventional H-bonding interactions at 2.8 – 3.1 Å. The hydrophobic side chains of Cys-44, Met-165, and Gln-192 form weak van der Waals interactions with asarinin. Interestingly, it has high GI absorption due to the presence of six H-bond acceptors in the moiety.

MM-PBSA calculation

After MD simulations, free energy methods can be used to obtain the binding free energy of protein-ligand complexes. Free energy methods are diverse and high accuracy for estimating Mpro with ligands. A total of 1000 snapshots were extracted evenly from the MD simulation. From the snapshots, energy of molecular mechanical (E_{MM}) and solvation accessible (PBSA) were calculated for our system. The energy terms of electrostatic, van der Waals (vdWs), polar and solvent accessible surface area and total binding energies were displayed in Fig. 8. The electrostatic, vdWs, and nonpolar solvation free energy are dominantly driving the binding energy. The polar solvation free energy destabilizes the binding interactions. The vdWs interactions predominantly enhance the binding energy between protein and ligands. Compounds sitosterol, spinasterol and asarinin possess stronger binding interactions with Mpro structure. The respective binding energy is -24.56, -26.07 and -25.76 kcal/mol obtained from MM/PBSA. Especially, asarinin shows higher vdW, electrostatic, and polar interactions with Mpro. The average binding energy for all the simulated complexes were plotted with time which is displayed in SI **Fig. S3.** The binding free energy plots of lupeol and glabridin complexes show large fluctuations and their binding energy is -21.08 and -18.17 kcal/mol, respectively. From the energy calculations, we concluded sitosterol, spinasterol and asarinin exhibit stronger interactions with Mpro.

Further, we calculated per-residue decomposition analysis to understand the contribution of specific amino acid interaction on binding free energy using MM-PBSA. Free energy decomposition analysis to identify the hot spot residues that participate in protein-ligand binding interactions. The hot spot residues are helpful to rational drug design of potent inhibitors to the drug target. We extracted 1000 snapshots for each system and the average ligand-residue interaction energies ($\Delta E_{lig-res}$) were calculated. The hot spot residue is defined by the residues that possess ($\Delta E_{lig-res}$) more than -1.0 kcal/mol, which is listed in Table 3. We considered the most significant hot spot residue is ($\Delta E_{lig-res} \geq$ -3.0 kcal/mol), and the common significant hot spot residues in ligand-protein are Thr-25, Met-49, Cys-145, Met-165, and Gln-189. These residues are constantly interacted with the ligands and make stronger H-bond and hydrophobic interactions. Mostly, asarinin has stronger interactions with Mpro residues. It forms stronger per-residue interactions of -6.7 and -7.7 kcal/mol with Met-49 and Met-165, respectively. Sitosterol, spinasterol and asarinin have stronger interactions with Mpro, and asarinin exhibits high GI absorption.

Table 3

Calculated ligand – residue MM-PBSA interactions energies (kcal/mol).[a]

Residue ID	Residue name	Sitosterol	Spinasterol	Lupeol	Glabridin	Asarinin
25	**Thr**	**-1.5**	**-3.5**	**-3.1**	**-1.8**	**-3.6**
27	Leu	-2.6	-2.0	-2.5	-2.6	-0.7
42	Val	-0.9	-1.2	-0.6	-0.4	-0.5
45	Cys	-0.0	-0.4	-0.2	-0.2	-1.7
46	Ser	-0.6	-1.4	-0.1	-0.1	-1.0
47	Glu	-0.6	-1.5	-0.9	-0.1	-0.6
48	Asp	-0.9	-1.5	-1.2	-0.3	-1.1
49	**Met**	**-4.1**	**-7.8**	**-3.7**	**-5.3**	**-6.7**
141	Leu	-0.7	-0.2	-1.4	-0.4	-0.1
145	**Cys**	**-1.1**	**-1.8**	**-1.6**	**-3.5**	**-1.2**
165	**Met**	**-4.4**	**-2.2**	**-3.1**	**-3.9**	**-7.7**
166	Glu	1.2	-1.3	0.1	-0.0	3.4
167	Leu	-0.5	-0.3	-0.4	-0.2	-2.4
168	Pro	-3.1	-0.2	-1.1	-0.0	-1.3
187	Asp	-1.2	-0.6	-1.1	0.3	-1.2
189	**Gln**	**-1.6**	**-1.5**	**0.1**	**-2.1**	**-3.8**
191	Ala	-1.2	-0.2	-0.0	-0.1	-0.5

[a] The common hot spot residues for all ligands are Thr-25, Met-49, Cys-145, Met-165 and Gln-189. (Highlighted in bold)

Conclusions

The contagious disease of SARS-CoV-2 spread worldwide, and the mortality rate also hikes. It is an urgent need to find potential antiviral drugs against SARS-CoV-2. CADD approaches are helpful to identify the potential drug against COVID-19. Available drugs cause adverse effect and their interaction mechanisms are still elusive. The selected phytochemicals from various herbal plants strongly interacted with the Mpro of SARS-CoV-2. We have selected 25 chemical compounds, which are involved in the apoptosis process and exhibit antiviral and anti-inflammatory activities. Molecular docking was used to screen the chemical compounds, according to their binding energies. ADME properties help to understand the drug-like properties of all chemical compounds. The five compounds whose binding affinities are greater than

-8.0 kcal/mol are selected for further screening where MD simulation was incorporated. As a result, protein-ligand complexes are maintained stable throughout the simulation time. Thereby, the stability was improved in the presence of chemical compounds. MM-PBSA calculation provided the binding free energy for all compounds. Compounds sitosterol, spinasterol, and asarinin show stronger interactions with Mpro of SARS-CoV-2. The most significant hot spot residues Thr-25, Met-49, Cys-145, Met-165, and Gln-189 are made important contributions on protein-ligand binding, which can help to drug design for target interactions of Mpro. We found out among these three compounds, the chemical scaffold of asarinin is attractive and the predicted GI absorption is high and made stronger interactions with Mpro. Chemical compounds from various herbal plants and foods were shown better antiviral activity for COVID-19. In conclusion, we screened the natural inhibitors, which is helpful to proceed with further drug development against the Mpro of SARS-CoV-2.

Declarations

Acknowledgments

K. P. thanks SRM Institute of Science and Technology (SRM-IST) Research Fellowship for his research work. M. P. thanks to the Department of Science and Technology-Science and Engineering Research Board (DST-SERB) (Grant number: ECR/2017/000891), New Delhi, India for the financial support. The authors also thank SRM-IST for providing the supercomputing facility and financial support.

Conflicts of Interest

There are no conflicts of interest to declare.

Data availability

The data are available from the corresponding author on reasonable request.

Code availability

Gaussian, Gromacs and Amber packages.

Author contributions

Kandhan Palanisamy: Formal analysis, Investigation, Methodology and Writing – original draft.

K. Rudharachari Maiyelvaganan and Shanmugasundaram Kamalakannan: Formal analysis, and Resources.

Ramasamy Thilagavathi and Chelliah Selvam: Validation, Visualization and Writing – review & editing.

Muthuramalingam Prakash: Conceptualization, Project administration, Supervision and Writing – review & editing.

References

1. Kuiken T, Fouchier RAM, Schutten M, et al (2003) Newly discovered coronavirus as the primary cause of severe acute respiratory syndrome. Lancet 362:263-270. https://doi.org/10.1016/S0140-6736(03)13967-0
2. Osterhaus ADME, Fouchier RAM, Zaki AM, Sander VB, Bestebroer TM (2012) Isolation of a Novel Coronavirus from a Man with Pneumonia in Saudi Arabia. N Engl J Med 367:1814-20. https://doi.org/10.1056/NEJMoa1211721
3. Lu H, Stratton CW, Tang YW (2020) Outbreak of pneumonia of unknown etiology in Wuhan, China: The mystery and the miracle. J Med Virol 92:401–402. https://doi.org/10.1002/jmv.25678
4. Sohrabi C, Alsafi Z, O'Neill N, et al (2020) World Health Organization declares global emergency: A review of the 2019 novel coronavirus (COVID-19). Int J Surg 76:71–76. https://doi.org/10.1016/j.ijsu.2020.02.034
5. Wei H, Yin H, Huang M, Guo Z (2020) The 2019 novel cornoavirus pneumonia with onset of oculomotor nerve palsy: a case study. J Neurol 267:1550–1553. https://doi.org/10.1007/s00415-020-09773-9
6. Maier HJ, Bickerton E, Britton P (2015) Coronaviruses: Methods and protocols. Coronaviruses Methods Protoc 1282:1–282. https://doi.org/10.1007/978-1-4939-2438-7
7. Gorbalenya AE, Baker SC, Baric RS, et al (2020) The species Severe acute respiratory syndrome-related coronavirus: classifying 2019-nCoV and naming it SARS-CoV-2. Nat Microbiol 5:536–544. https://doi.org/10.1038/s41564-020-0695-z
8. Ankit B. Patel (2020) COVID-19 and Angiotensin-Converting Enzyme Inhibitors and Angiotensin Receptor Blockers What Is the Evidence? JAMA 02115. https://doi.org/10.1038/nm1267
9. Forster P, Forster L, Renfrew C, Forster M (2020) Phylogenetic network analysis of SARS-CoV-2 genomes. Proc Natl Acad Sci 117:9241-9243. https://doi.org/10.1073/pnas.2004999117
10. Liu C, Zhou Q, Li Y, et al (2020) Research and Development on Therapeutic Agents and Vaccines for COVID-19 and Related Human Coronavirus Diseases. ACS Cent Sci 6:315-331. https://doi.org/10.1021/acscentsci.0c00272
11. Hosseini-zare MS, Selvam C (2020) Coronavirus (SARS-CoV-1) with structurally diverse. RSC adv 10:28287–28299. https://doi.org/10.1039/d0ra04395h
12. Callaway E (2020) Making sense of coronavirus mutations. Nature 585:174–177.
13. Pillaiyar T, Manickam M, Namasivayam V, et al (2016) An overview of severe acute respiratory syndrome-coronavirus (SARS-CoV) 3CL protease inhibitors: Peptidomimetics and small molecule chemotherapy. J Med Chem 59:6595–6628. https://doi.org/10.1021/acs.jmedchem.5b01461
14. Francés-Monerris A, Hognon C, Miclot T, et al (2020) Molecular Basis of SARS-CoV-2 Infection and Rational Design of Potential Antiviral Agents: Modeling and Simulation Approaches. J Proteome Res 19:4291-4315. https://doi.org/10.1021/acs.jproteome.0c00779

15. Jin Z, Du X, Xu Y, et al (2020) Structure of Mpro from SARS-CoV-2 and discovery of its inhibitors. Nature 582:289–293. https://doi.org/10.1038/s41586-020-2223-y
16. Ullrich S, Nitsche C (2020) The SARS-CoV-2 main protease as drug target. Bioorganic Med Chem Lett 30:127377. https://doi.org/10.1016/j.bmcl.2020.127377
17. Gautret P, Lagier JC, Parola P, et al (2020) Hydroxychloroquine and azithromycin as a treatment of COVID-19: results of an open-label non-randomized clinical trial. Int J Antimicrob Agents 56:105949. https://doi.org/10.1016/j.ijantimicag.2020.105949
18. Parvathaneni V, Gupta V (2020) Utilizing drug repurposing against COVID-19 – Efficacy, limitations, and challenges. Life Sci 259:118275. https://doi.org/10.1016/j.lfs.2020.118275
19. Quek P. Medicinal Plants Research in Asia. 2004.
20. Islam MT, Sarkar C, El-kersh DM, Jamaddar S (2020) Natural products and their derivatives against coronavirus: A review of the non-clinical and pre-clinical data. Phytotherapy Research 34:2471-2492. https://doi.org/10.1002/ptr.6700
21. My TTA, Loan HTP, Hai NTT, et al (2020) Evaluation of the Inhibitory Activities of COVID-19 of Melaleuca cajuputi Oil Using Docking Simulation. ChemistrySelect 5:6312–6320. https://doi.org/10.1002/slct.202000822
22. Kumar R, Piya G, Mudgal P, et al (2015) Herbal plants and plant preparations as remedial approach for viral diseases. VirusDisease 26:225-236. https://doi.org/10.1007/s13337-015-0276-6
23. Kumar S, Sharma PP, Shankar U, et al (2020) Discovery of New Hydroxyethylamine Analogs against 3CL pro Protein Target of SARS-CoV-2: Molecular Docking, Molecular Dynamics Simulation, and Structure–Activity Relationship Studies . J Chem Inf Model 60:5754-5770. https://doi.org/10.1021/acs.jcim.0c00326
24. Gahlawat A, Kumar N, Kumar R, et al (2020) Structure-Based Virtual Screening to Discover Potential Lead Molecules for the SARS-CoV-2 Main Protease. J Chem Inf Model 60:5781-5793. https://doi.org/10.1021/acs.jcim.0c00546
25. Singam ERA, Merrill MA La, Durkin KA, Smith MT (2020) Structure-Based Virtual Screening of a Natural Product Database to Identify Several Possible SARS-CoV-2 Main Protease Inhibitors. ChemRxiv
26. Thi B, Thuy P, Thi T, et al (2020) Investigation into SARS-CoV - 2 Resistance of Compounds in Garlic Essential Oil. ACS Omega 5:8312-8320. https://doi.org/10.1021/acsomega.0c00772
27. Kulkarni SA, Nagarajan SK, Ramesh V, et al (2020) Computational evaluation of major components from plant essential oils as potent inhibitors of SARS-CoV-2 spike protein. J Mol Struct 1221:128823. https://doi.org/10.1016/j.molstruc.2020.128823
28. Gutierrez-Villagomez JM, Campos-García T, Molina-Torres J, et al (2020) Alkamides and Piperamides as Potential Antivirals against the Severe Acute Respiratory Syndrome Coronavirus 2 (SARS-CoV-2). J Phys Chem Lett 11:8008–8016. https://doi.org/10.1021/acs.jpclett.0c01685
29. Palanisamy K, Rubavathy SME, Prakash M, et al (2022) Antiviral activities of natural compounds and ionic liquids to inhibit the Mpro of SARS-CoV-2 : a computational approach. RSC Adv 12:3687–3695.

https://doi.org/10.1039/D1RA08604A

30. Wu D, Koganti R, Lambe UP, et al (2020) Vaccines and Therapies in Development for SARS-CoV-2 Infections. J Clin Med 9:1885. https://doi.org/10.3390/jcm9061885
31. Linlin Z, Daizong L, Xinyuanyuan S, Ute C, Christian D, Lucie S, Stephan B, Katharina R, Rolf H (2020) Crystal structure of SARS-CoV-2 main protease provides a basis for design of improved α-ketoamide inhibitors. Science 368:409-412. https://doi.org/ 10.1126/science.abb3405
32. Frisch MJ, Trucks GW, Schlegel HB, et al. Gaussian 16, revision A. 03. Wallingford CT. 2016.
33. Meng X, Zhang H, Mezei M, Cui M (2011) Molecular Docking : A Powerful Approach for Structure-Based Drug Discovery. Curr Comput Aided Drug Des 7;146–157. https://doi.org/10.2174/157340911795677602
34. Garrett MM, Ruth H, William L, Michel FS, Richard KB, David SG, Arthur J. Olson (2012) AutoDock4 and AutoDockTools4: Automated Docking with Selective Receptor Flexibility. J Comput Chem 32:174–182. https://doi.org/10.1002/jcc
35. Daina A, Michielin O, Zoete V (2017) SwissADME: A free web tool to evaluate pharmacokinetics, drug-likeness and medicinal chemistry friendliness of small molecules. Sci Rep 7:1–13. https://doi.org/10.1038/srep42717
36. Pires DEV, Blundell TL, Ascher DB (2015) pkCSM: Predicting small-molecule pharmacokinetic and toxicity properties using graph-based signatures. J Med Chem 58:4066–4072. https://doi.org/10.1021/acs.jmedchem.5b00104
37. Lindorff-Larsen K, Piana S, Palmo K, et al (2010) Improved side-chain torsion potentials for the Amber ff99SB protein force field. Proteins Struct Funct Bioinforma 78:1950–1958. https://doi.org/10.1002/prot.22711
38. Wang J, Wolf RM, Caldwell JW, et al (2004) Development and Testing of a General Amber Force Field. J Comput Chem 56531:1157–1174. https://doi.org/10.1002/jcc.20035
39. Sousa Da Silva AW, Vranken WF (2012) ACPYPE - AnteChamber PYthon Parser interfacE. BMC Res Notes 5:1–8. https://doi.org/10.1186/1756-0500-5-367
40. Bayly CI, Cieplak P, Cornell WD, Kollman PA (1993) A well-behaved electrostatic potential based method using charge restraints for deriving atomic charges: The RESP model. J Phys Chem 97:10269–10280. https://doi.org/10.1021/j100142a004
41. Berendsen HJC, van der Spoel D, van Drunen R (1995) GROMACS: A message-passing parallel molecular dynamics implementation. Comput Phys Commun 91:43–56. https://doi.org/10.1016/0010-4655(95)00042-E
42. Kumari R, Kumar R, Lynn A (2014) G-mmpbsa -A GROMACS tool for high-throughput MM-PBSA calculations. J Chem Inf Model 54:1951–1962. https://doi.org/10.1021/ci500020m
43. L DeLano W (2020) Pymol: An open-source molecular graphics tool. Protein Crystallogr 40.
44. Ricker EW (1954) VMD: Visual Molecular Dynamics. J Fish Res Board Canada 11:559–623. https://doi.org/10.1016/0263-7855(96)00018-5

45. Mengist HM, Fan X, Jin T (2020) Designing of improved drugs for COVID-19: Crystal structure of SARS-CoV-2 main protease Mpro. Signal Transduct Target Ther 5:2–3. https://doi.org/10.1038/s41392-020-0178-y
46. Nguyen NT, Nguyen TH, Pham TNH, et al (2020) Autodock Vina Adopts More Accurate Binding Poses but Autodock4 Forms Better Binding Affinity. J Chem Inf Model. 60:204–211. https://doi.org/10.1021/acs.jcim.9b00778
47. Huynh T, Wang H, Luan B (2020) In Silico Exploration of the Molecular Mechanism of Clinically Oriented Drugs for Possibly Inhibiting SARS-CoV-2's Main Protease. J Phys Chem Lett 11:4413–4420. https://doi.org/10.1021/acs.jpclett.0c00994
48. Peele KA, Potla Durthi C, Srihansa T, et al (2020) Molecular docking and dynamic simulations for antiviral compounds against SARS-CoV-2: A computational study. Informatics Med Unlocked 19:100345. https://doi.org/10.1016/j.imu.2020.100345
49. Srinivasan K (2007) Black pepper and its pungent principle-piperine: A review of diverse physiological effects. Crit Rev Food Sci Nutr 47:735–748. https://doi.org/10.1080/10408390601062054
50. Zaveri M, Khandhar A, Patel S, Patel A (2010) Chemistry and pharmacology of Piper longum L. Int J Pharm Sci Rev Res 5:67–76
51. Lee HS, Koo YC, Suh HJ, et al (2010) Preventive effects of chebulic acid isolated from Terminalia chebula on advanced glycation endproduct-induced endothelial cell dysfunction. J Ethnopharmacol 131:567–574. https://doi.org/10.1016/j.jep.2010.07.039
52. Laphookhieo S, Phungpanya C, Tantapakul C, et al (2011) Chemical Constituents from Aegle marmelos. J. Braz. Chem Soc 22:176–178
53. Sahu J, Rathi B, Koul S, Khosa RL (2013) Solanum trilobatum (Solanaceae) - an overview. J Nat Remedies 13:76–80. https://doi.org/10.18311/jnr/2013/100
54. Kaur R, Kaur H, Dhindsa AS (2013) Glycyrrhiza glabra: a phytopharmacological review. Int J Pharm Sci Res 4:2470–2477. https://doi.org/10.13040/IJPSR.0975-8232.4(7).2470-77
55. Lipinski CA, Lombardo F, Dominy BW, Feeney PJ (2012) Experimental and computational approaches to estimate solubility and permeability in drug discovery and development settings. Adv Drug Deliv Rev 64:4–17. https://doi.org/10.1016/j.addr.2012.09.019
56. Ad ABAW, Downie AC, Fink CS (2020) Inhibition of growth and stimulation of apoptosis by ß-sitosterol treatment of MDA-MB-231 human breast cancer cells in culture. Int J Mol Med 5:541–545. https://doi.org/10.3892/ijmm.5.5.541
57. Velazco O, Chamorro G (2005) Genotoxic and Cytotoxic Studies of Beta-Sitosterol and Pteropodine in Mouse 3:242–247. https://doi.org/10.1155/JBB.2005.242
58. Saeidnia S, Manayi A, Gohari AR (2014) The Story of Beta-sitosterol- A Review. European Journal of Medicinal Plants 4:590–609. https://doi.org/ 10.9734/EJMP/2014/7764
59. Meneses-Sagrero SE, Navarro-Navarro M, Ruiz-Bustos E, et al (2017) Antiproliferative activity of spinasterol isolated of Stegnosperma halimifolium. Saudi Pharm J 25:1137–1143.

https://doi.org/10.1016/j.jsps.2017.07.001

60. Sedky NK, El Gammal ZH, Wahba AE, et al (2018) The molecular basis of cytotoxicity of α-spinasterol from Ganoderma resinaceum: Induction of apoptosis and overexpression of p53 in breast and ovarian cancer cell lines. J Cell Biochem 119:3892–3902. https://doi.org/10.1002/jcb.26515
61. Flekhter OB, Boreko EI, Nigmatullina LR, et al (2004) Synthesis and antiviral activity of lupane triterpenoids and their derivatives. Pharm Chem J 38:355–358. https://doi.org/10.1023/B:PHAC.0000048431.65649.bd
62. Saleem M (2009) Lupeol, a novel anti-inflammatory and anti-cancer dietary triterpene. Cancer Lett 285:109–115. https://doi.org/10.1016/j.canlet.2009.04.033
63. Fukai T, Satoh K, Nomura T, Sakagami H (2003) Preliminary evaluation of antinephritis and radical scavenging activities of glabridin from Glycyrrhiza glabra. Fitoterapia. 74:624–629. https://doi.org/10.1016/S0367-326X(03)00164-3
64. Wang L, Yang R, Yuan B, et al (2015) The antiviral and antimicrobial activities of licorice, a widely-used Chinese herb. Acta Pharm Sin B 5:310–315. https://doi.org/10.1016/j.apsb.2015.05.005
65. Jeong M, Kim HM, Lee JS, et al (2018) (−)-Asarinin from the roots of asarum sieboldii induces apoptotic cell death via caspase activation in human ovarian cancer cells. Molecules. 23:1849. https://doi.org/10.3390/molecules23081849

Figures

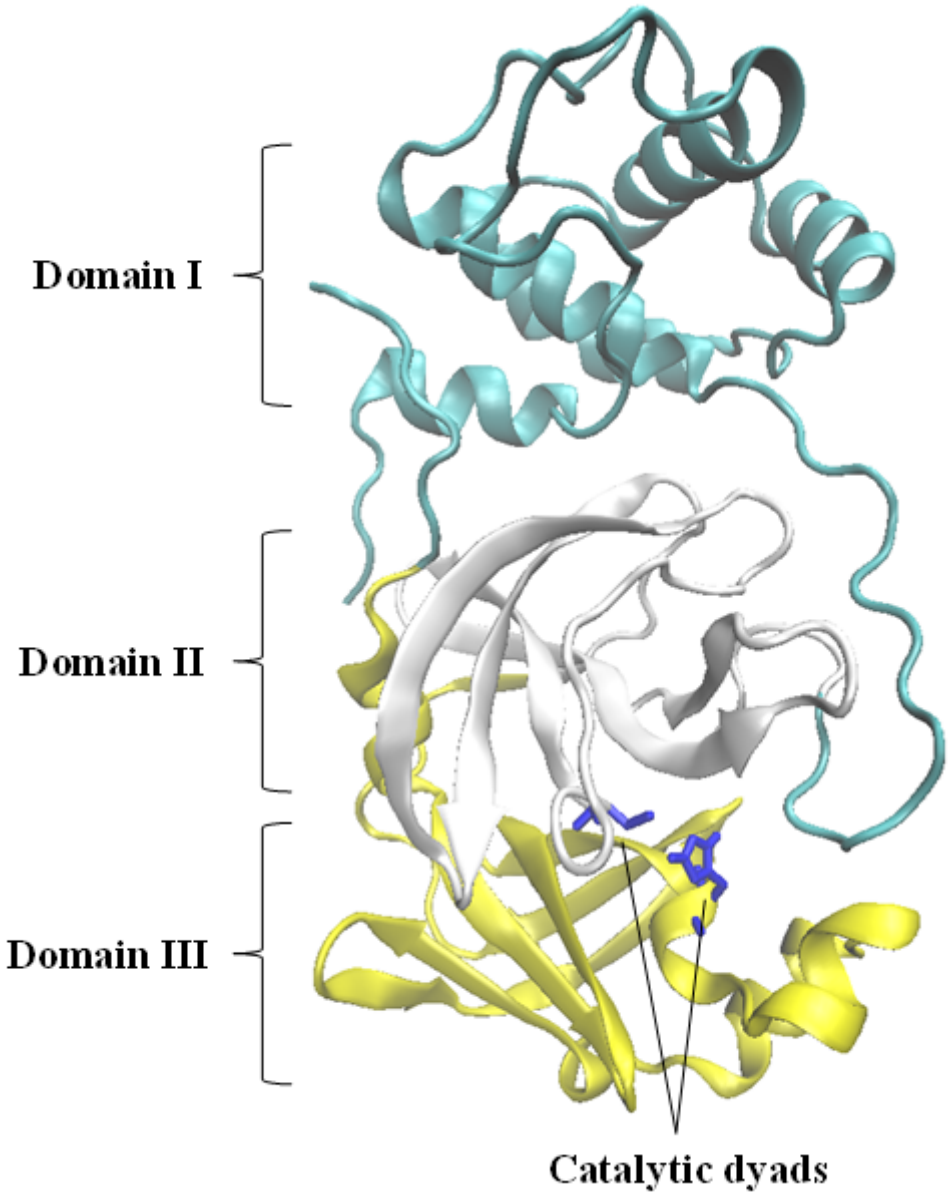

Figure 1

Cartoon representations of Mpro, domain I, domain II and domain III are shown in different colors. (Catalytic dyads of Cys-145 and His-41 are shown in blue color).

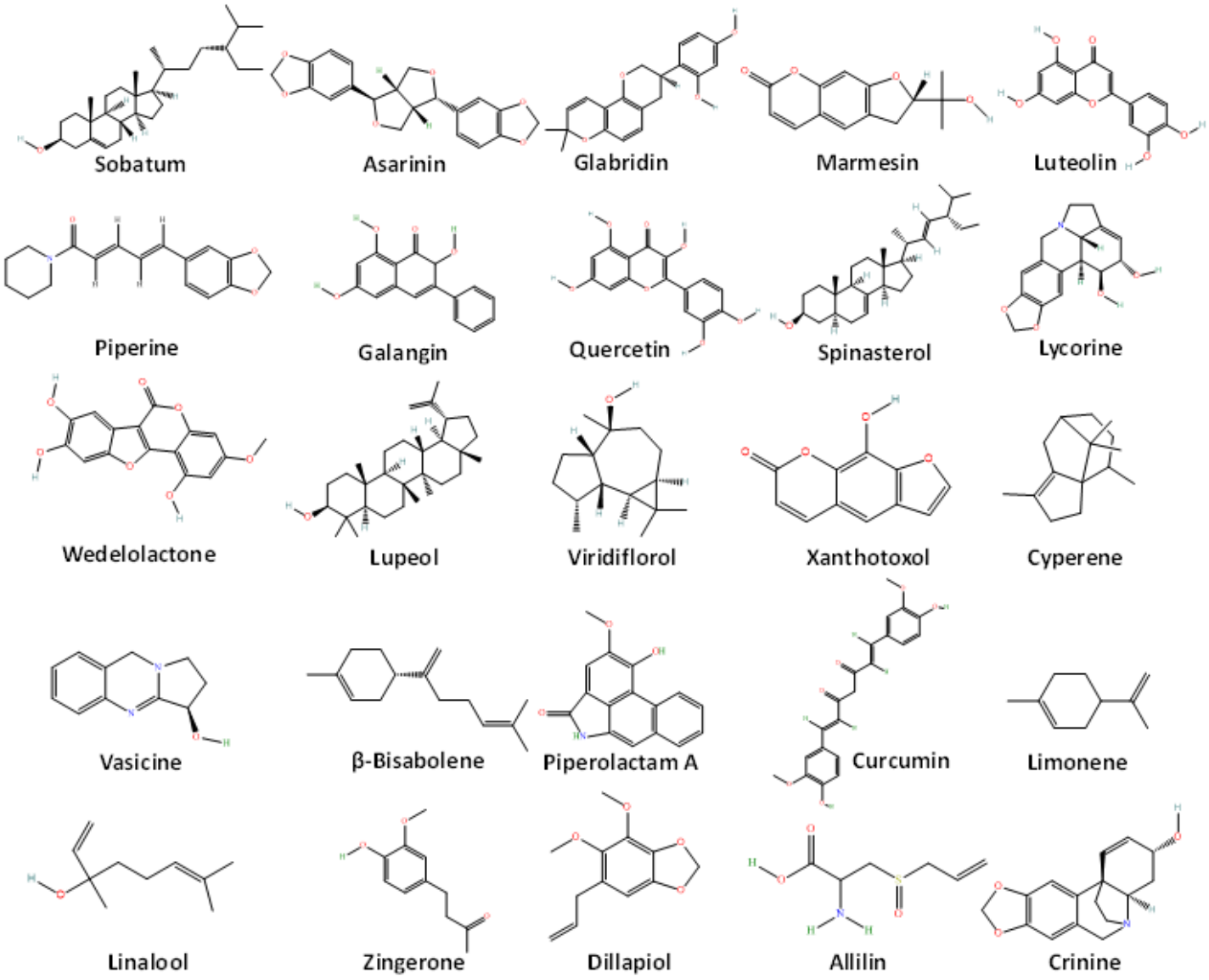

Figure 2

Two dimensional structures of selected chemical compounds are shown.

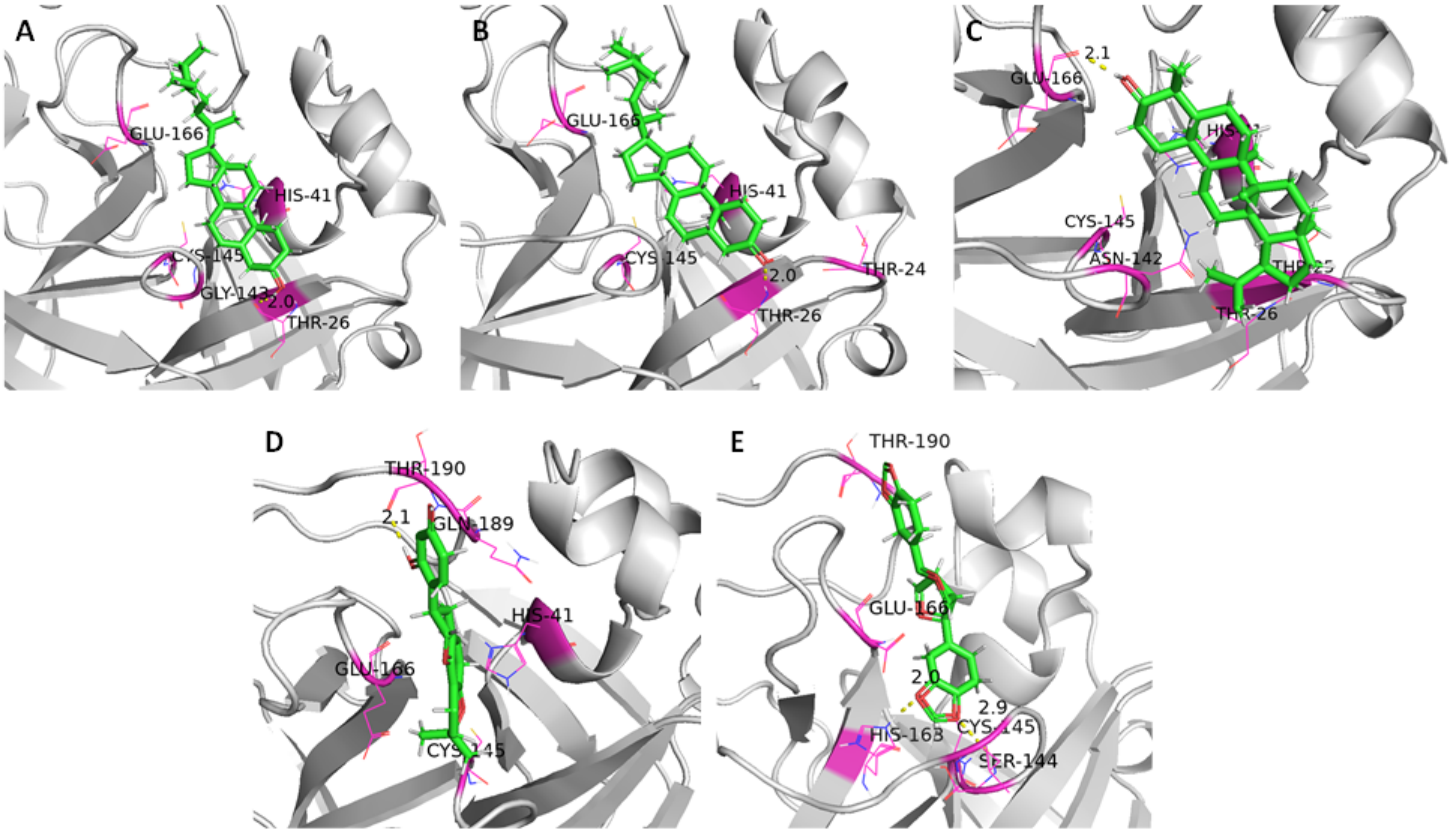

Figure 3

Docking conformations of SARS-CoV-2 Mpro with A) Sitosterol B) Spinasterol C) Lupeol D) Glabridin and E) Asarinin.

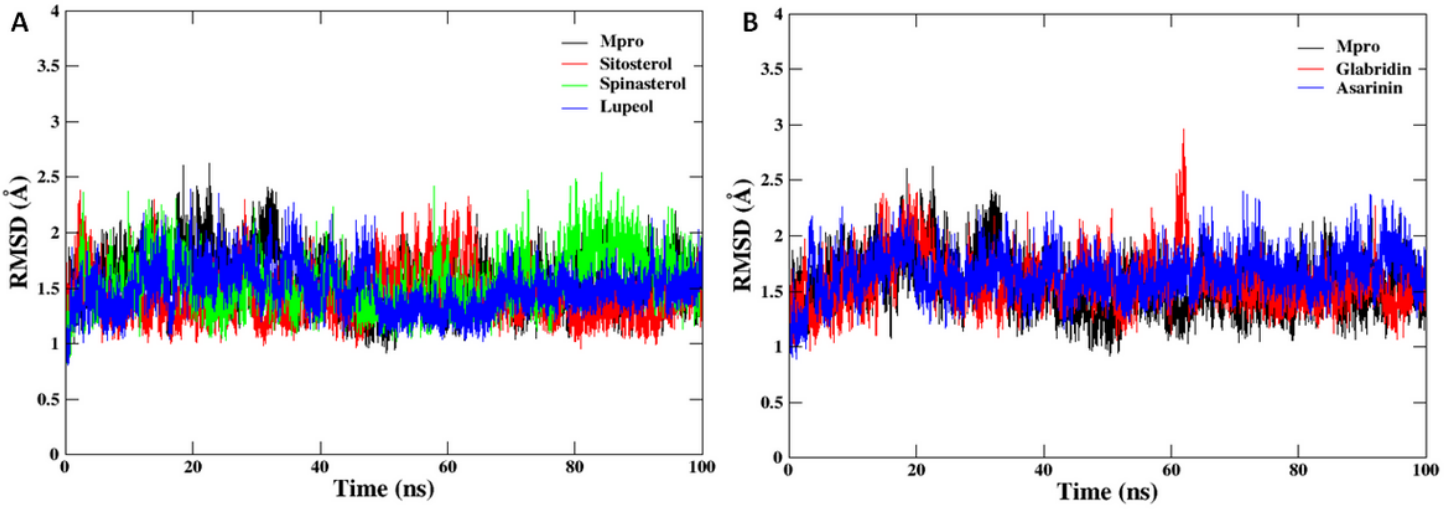

Figure 4

RMSD plots of A) Mpro-apo, Mpro-sitosterol, Mpro-spinasterol, Mpro-lupeol and B) Mpro-apo, Mpro-glabridin and Mpro-asarinin plotted against with simulation time.

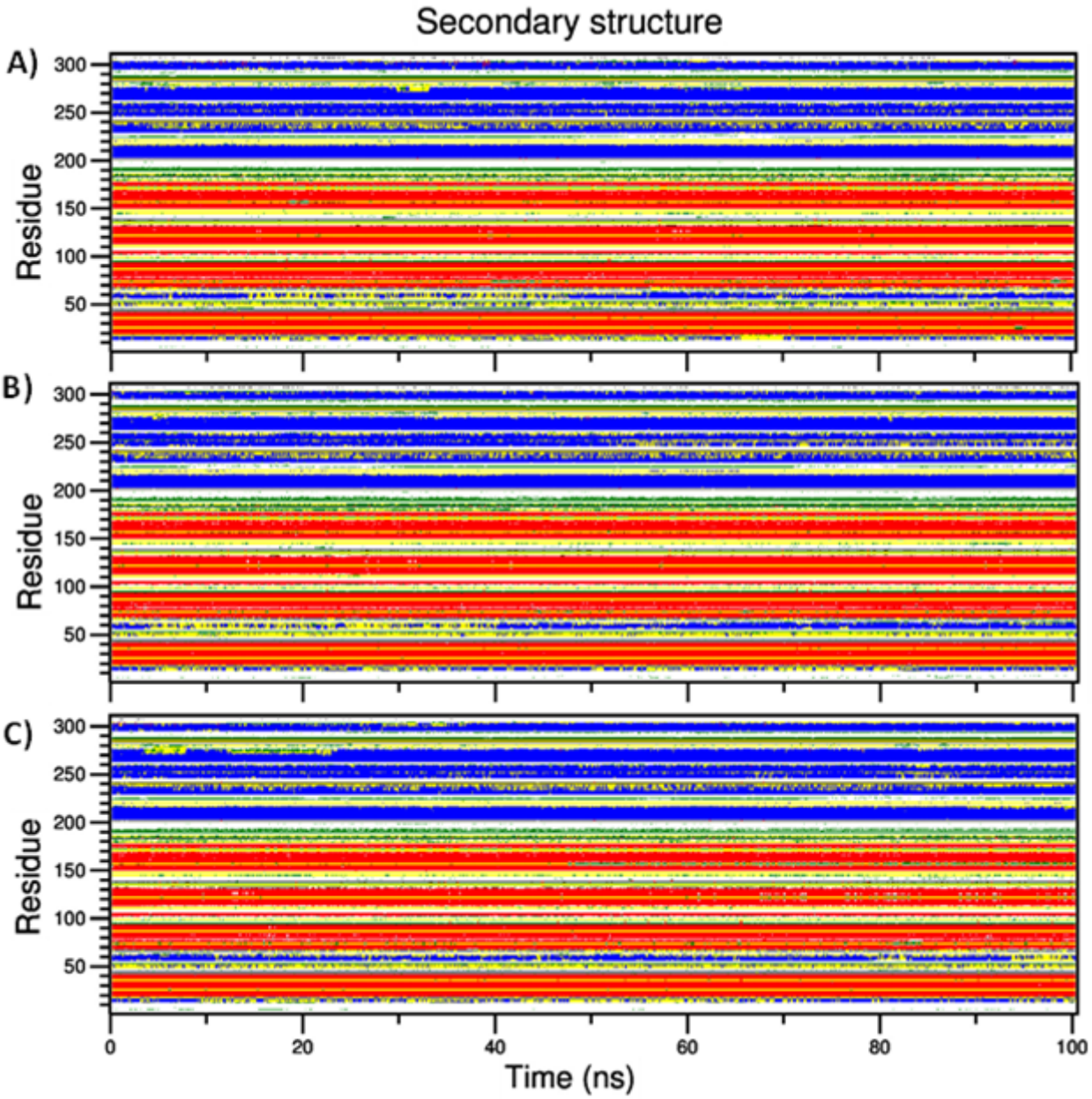

Figure 5

The secondary structure analysis of A) Sitosterol B) Spinasterol and C) Asarinin are shown.

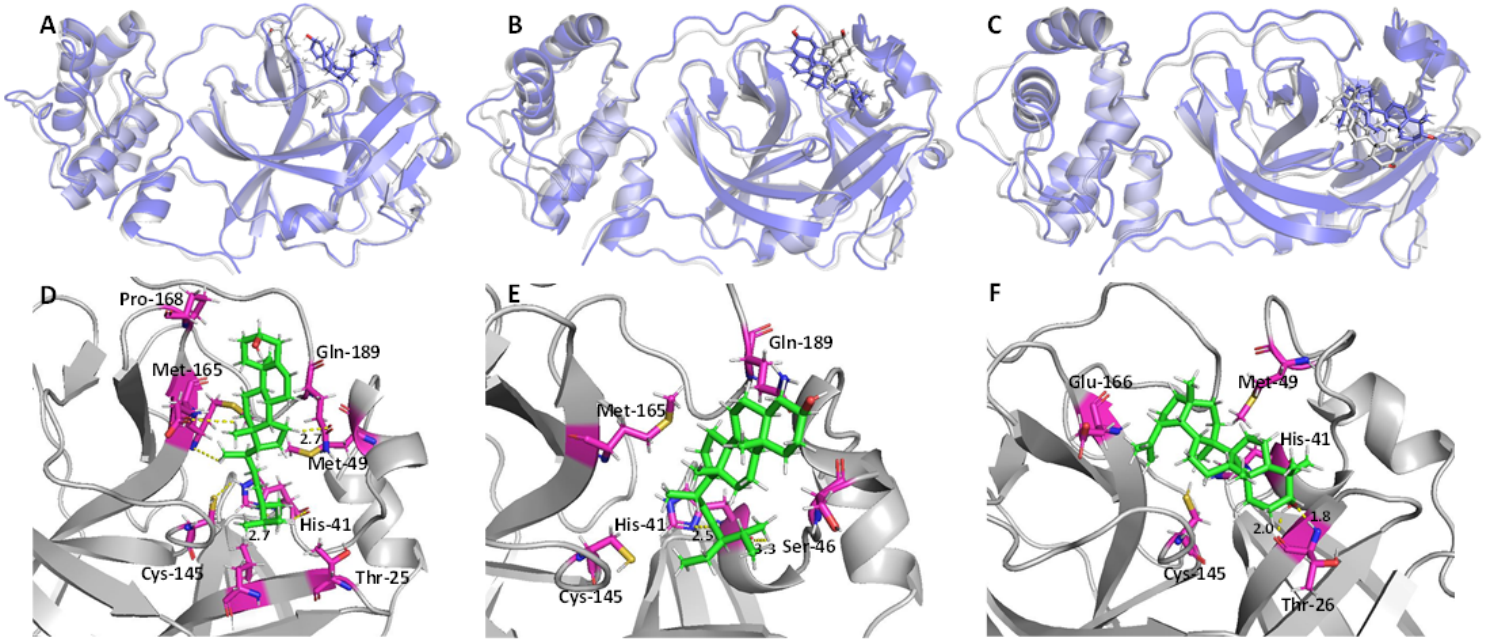

Figure 6

Superimpositions of crystal structures (grey) and MD equilibrated systems (blue) of SARS-CoV-2 Mpro with three ligands A) sitosterol B) spinasterol and C) lupeol. The detailed ligand-residue complexes interactions are shown in D-E. The hot spot residues are ($\Delta E_{lig\text{-}res} \geq$ -3.0 kcal/mol) labeled in pink color and ligands are shown in green color.

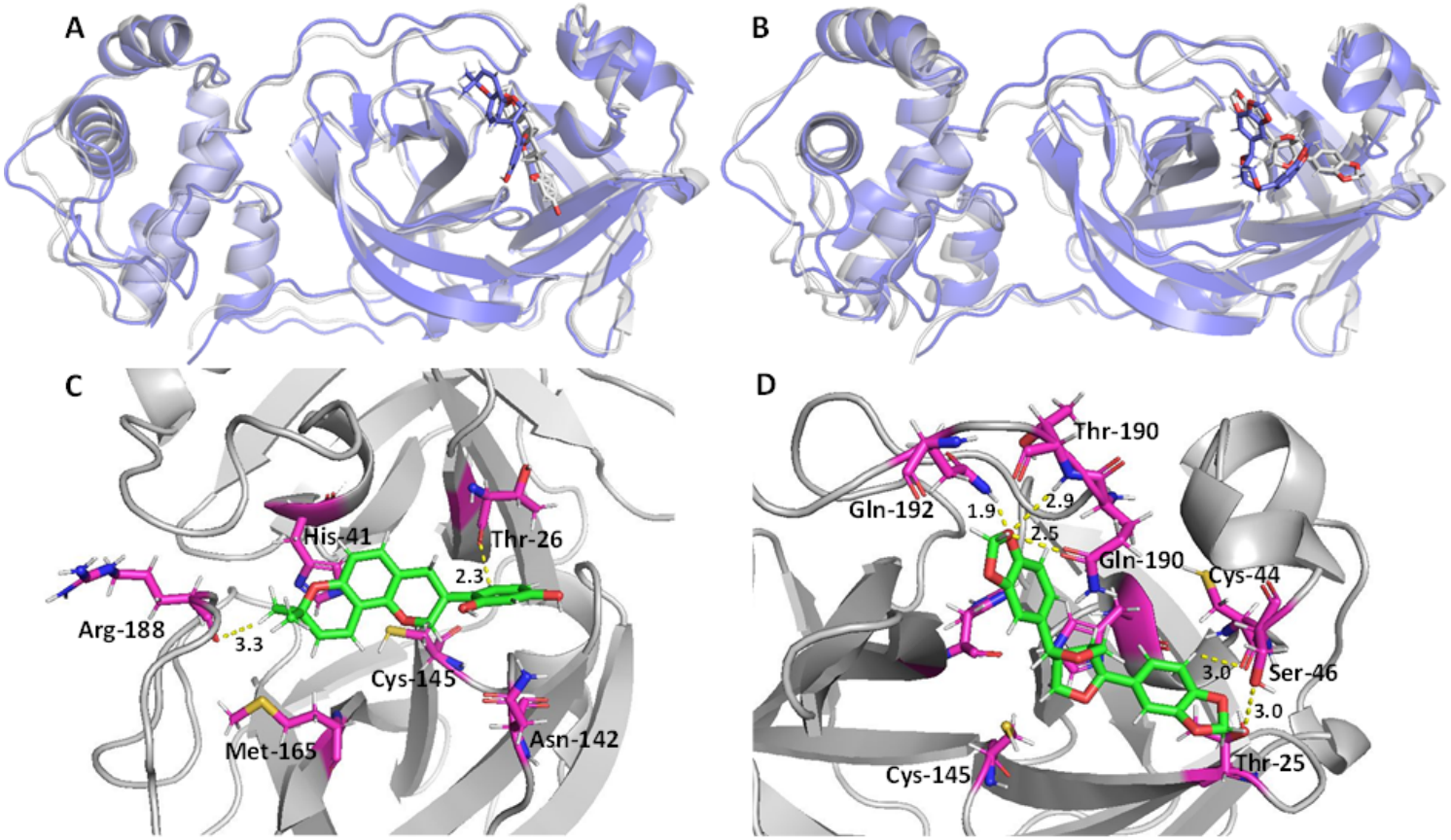

Figure 7

Superpositions of crystal structures (grey) and MD equilibrated systems (blue) of SARS-CoV-2 Mpro with three ligands A) glabridin and B) asarinin. The detailed ligand-residue interactions of complexes are shown in C and D. The hot spot residues are ($\Delta E_{lig\text{-}res} \geq$ -3.0 kcal/mol) labeled in pink color and ligands are shown in green color.

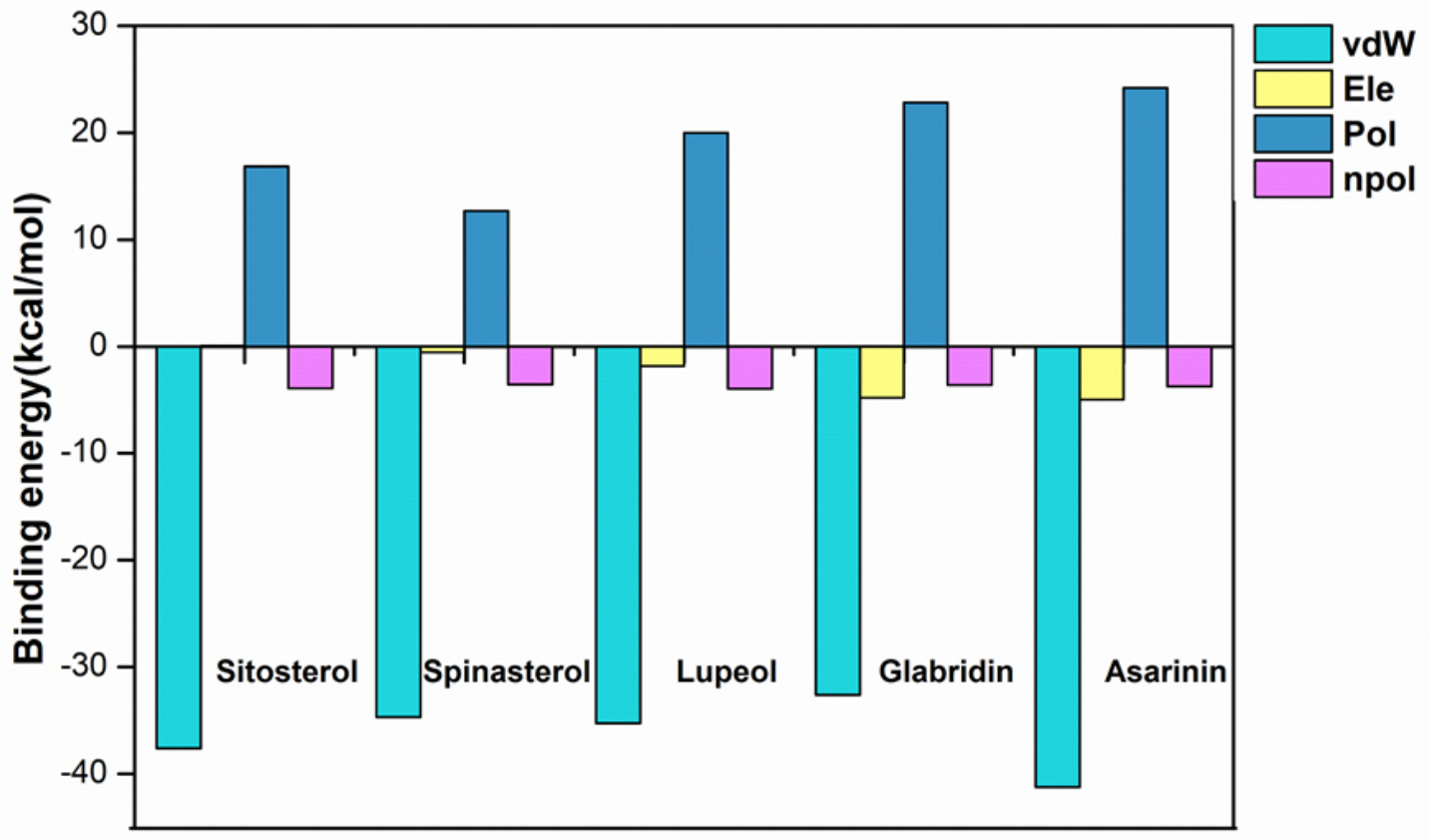

Figure 8

Calculated MM-PBSA binding energies of potential inhibitors with Mpro of SARS-CoV-2. vdW = van der Walls, Ele = Electrostatic, Pol = Polar solvation and npol = non polar solvation free energies are shown.

Supplementary Files

This is a list of supplementary files associated with this preprint. Click to download.

- GA.png
- SIJMolMod.docx